Sensors & Actuators: B. Chemical 389 (2023) 133866

Contents lists available at ScienceDirect

Sensors and Actuators: B. Chemical

journal homepage: www.elsevier.com/locate/snb

Compact methane sensor using an integrating sphere and interband cascade laser at 3313 nm

Nicholas M. Davis, Daniel Francis, Jane Hodgkinson *, Ralph P. Tatam

Engineering Photonics, Cranfield University, Cranfield, Bedfordshire, MK43 0AL, UK

ARTICLE INFO

Keywords:
Integrating sphere
Gas detection
Interband cascade laser
Atmospheric methane
Tunable diode laser absorption spectroscopy
TDLAS

ABSTRACT

We present a sensor for gas detection utilising an integrating sphere and interband cascade laser for tunable diode laser absorption spectroscopy (TDLAS). Measurements were made of the methane absorption line at 3313 nm using an integrating sphere with an effective pathlength of 70.1 cm. Gas concentrations were estimated from normalised absorption spectra with line fitting to 7 absorption lines within the scan. Testing showed that measurements were linear for methane in synthetic air for concentrations in the range 0–50 ppm. With an averaging time of 20 s, the noise-equivalent methane concentration was 180 ppb (1σ). The system requires minimal alignment, with preliminary measurements indicating the system is insensitive to vibration and misalignment of the laser input. The lack of alignment optics also allows it to be compact (190×170×120mm) and robust.

1. Introduction

Average global concentrations of greenhouse gases increased at a rate of 2.2 % per year between 2000 and 2010 [1], with current concentrations of CO_2, CH_4 and N_2O exceeding any level for the past 800,000 years, the period of measurement covered by ice cores [2].

The second of these gases, methane, is a colourless, odourless gas that can be found extensively in nature, being the most abundant organic trace gas in the atmosphere [3]. Although the concentration for methane is significantly lower than that of carbon dioxide (1.8 ppm compared with 410 ppm in 2019 [4]) it has a global warming potential up to 34 times greater than that of CO_2 over a hundred year period and much more (86 times greater) over its lifetime in the atmosphere of 20 years [5]. As a result, trace gas detection has attracted significant attention for environmental monitoring, with methane detection systems gaining increased focus.

Sensors based on the use of tunable diode laser absorption spectroscopy (TDLAS) provide a high specificity to the target gas, a fast response time, repeatable measurements and provide low limits of detection [6]. Measurements of optical absorption made in the mid IR region of the spectrum are able to access spectral features associated with fundamental vibrational transitions of molecular bonds, which for methane lie around 3.3 μm and 7.8 μm. These can be 100x stronger than their counterparts in the near IR that correspond to weaker overtone transitions.

Interband Cascade Lasers (ICLs) fill an important gap between the wavelength coverage of standard laser diodes and Quantum Cascade Lasers (QCLs), having an operating range between 3 and 6 μm. This presents the opportunity to make measurements at the fundamental absorption bands of a number of C-H, N-H and O-H molecules [6]. Difference Frequency Generation (DFG) sources and QCLs are also available in the mid infrared, however they each have disadvantages compared with ICLs. DFG sources are more complex than ICLs and can be sensitive to misalignment, whilst QCLs are noisier and not currently available in the 3–4 μm region.

Previous researchers have used a number of different techniques to obtain low limit of detection measurements for methane using ICLs as the source. A system using wavelength modulation spectroscopy (WMS) with a 16 m multipass gas cell was utilised by Song et al. to achieve a limit of detection of 5.84 ppb with a 2 s averaging time [7], with Xia et al. having achieved a limit of detection of 560 ppt at an averaging time of 290 s with a 580 m multipass cell using the same technique [8]. Although these systems produced high quality results in a laboratory environment, both utilised multipass cells that required high-precision alignment that would not be suitable in an environment with high vibration levels that could cause misalignment.

Alternatively, a quartz enhanced photoacoustic sensor (QEPAS) system used by Sampaolo et al. achieved a limit of detection of 90 ppb

* Corresponding author.
E-mail address: j.hodgkinson@cranfield.ac.uk (J. Hodgkinson).

https://doi.org/10.1016/j.snb.2023.133866
Received 20 October 2022; Received in revised form 27 March 2023; Accepted 20 April 2023
Available online 23 April 2023

with a 1 s averaging time [9]. QEPAS-based sensors are modular, rugged, highly portable, can operate in real-time and are wavelength-independent. However, one of the main limitations with this technique is the sensor's ability to detect specific gas components in a fluctuating background, such as those found in environmental monitoring [10].

Manfred et al. have achieved a 3 ppb limit of detection with an optical feedback cavity-enhanced absorption spectroscopy based system with an effective pathlength of 960 m and averaging time of 2 s [11]. The pathlengths of these systems, however, are sensitive to small fluctuations in mirror alignment and surface imperfections. As a result, instruments undergoing field trials using this technology require mechanical stability, dust-isolation and temperature and humidity management.

Multipass gas cells are used to achieve greater sensitivity by increasing the pathlength of a system [12]. These cells utilise mirrors of various sizes, curvature, and distance to produce multiple reflections of the incident beam, generating a longer pathlength in a relatively small volume, with the most common versions of these cells being the White cell [13] and Herriot cell [14].

The White cell consists of three spherical concave mirrors with the same curvature of radius, two closely spaced at one end of the cell with the third mirror opposite. By adjusting the separation distance between the two closely spaced mirrors symmetrically around the third mirror and its centre of curvature, the number of traversals (and therefore pathlength) can be adjusted. White cells are still commonly used in absorption spectroscopy for a number of reasons: the number of traversals is easily controlled and consequently so is the optical pathlength, beams of high numerical aperture can be used, and they are relatively stable. Pathlengths of several thousand metres can be achieved with this cell, with Ferguson et al. achieving a pathlength of 5984 m [15].

The Herriott cell operates using a similar technique to the White cell, except two mirrors are used instead of three. Light from a source is passed through a hole in one of the mirrors and reflected between the two. The beam can then either output back through the same hole or through a separate hole on the opposite mirror. The optical pathlength of the cell is controlled by changing the separation of the mirrors, making this cell simpler to align and operate than the White cell. The cell is also less susceptible to mechanical disturbance or vibration than the White cell and can be more stable [6]. Pathlengths of 10s of metres are typically achieved with these cells, with Li et al. utilising a 100 m cell in 2016 [16]. However, high numerical aperture beams cannot be utilised and the pathlength of the cell is limited by the number of reflection spots on the mirrors, as to avoid interference these spots cannot overlap [17].

The mirrors used in these cells also require precision manufacturing [18] and may be sensitive to degradation resulting from humidity or cleaning processes. Additionally, conventional multipass cells can suffer from the formation of etalons both inside the cell and from any windows present, resulting in a lower than expected improvement in signal to noise ratio from the increased pathlength [19]. The alignment processes involved in minimising these effects whilst achieving a long pathlength are often time consuming, with the optical alignment often sensitive to external environmental factors, such as vibration or thermal expansion/contraction.

Originally used for the measurement of the total flux of light sources, integrating spheres have also gained attention as multipass absorption cells [20]. One advantage is that they are understood to be tolerant to slight changes to alignment and vibration when used to measure absorption [20]. These spheres consist of a hollow cavity with a diffusely reflective internal surface. Typically, there are two or more ports for light sources and detectors as well as two ports for gas inflow and exhaust. To prevent direct illumination of the detector by the light source, a light barrier (or baffle) is often used. Integrating spheres have been shown to increase effective pathlength [21], both theoretically and experimentally, within a relatively small volume without the need for precise alignment, and are tolerant to misalignment in use. Previous work has shown a Zenith™ coated sphere with 101.6 cm internal diameter has an effective pathlength of 3.4 m at 1651 nm [22] and Hawe et al. have demonstrated a 2-inch diameter, Spectralon sphere with an effective pathlength of 114.7 cm at 1570 nm [23].

In this paper, the detection of methane at 3.3 μm using an ICL and gold-coated integrating sphere has been demonstrated for the first time. It has long been claimed that integrating spheres are tolerant to misalignment and vibration. Here, we show experimental verification of this, whilst also demonstrating an improvement in the noise level when vibration is applied. The sensor system was designed for installation and use on a light aircraft, where it would be subject to high levels of vibration and g-loading, making the use of an integrating sphere attractive.

2. Tunable diode laser spectroscopy of methane

The basic principle of optical absorption spectroscopy can be described using the Beer-Lambert law [24]:

$$I = I_0 \exp(-\alpha \ell) \tag{1}$$

where I is the light transmitted through the gas cell, I_0 is the light incident on the gas cell, α is the absorption coefficient of the target gas species (typically with units cm^{-1}) and ℓ is the cell's optical pathlength (typically with units cm). The value of α is equal to εc, where ε is the specific absorptivity of the gas (units cm^{-1} atm^{-1}) and c is the gas concentration (typically in units of partial pressure, atm). For low $\alpha\ell$, this equation becomes linear and can be expressed as follows:

$$\frac{\Delta I}{I_0} \approx \alpha \ell \tag{2}$$

Where $\Delta I = I_0 - I$ and $\Delta I/I_0$ is defined as the absorbance, which is unitless but often expressed in terms of absorbance units (AU). The limit of detection of a target gas species can be quantified as the noise equivalent absorbance (NEA, in units AU) or the minimum detectable absorption coefficient (α_{min} in cm^{-1}), allowing instrumental techniques to be compared without reference to the specific target gas.

Fig. 1 displays the absorption spectrum for methane in the near and mid-infrared. Due to the price and availability of components, many TDLAS based systems for detection of methane make use of the 1650 nm absorption region. However, as can be observed from this diagram, the strength of the methane absorption lines in this region are around 100 times smaller than those seen in the wavelength region around 3300 nm. The development of ICLs has allowed the measurement of gas absorption lines in the mid-infrared to take place, without the noise or alignment issues associated with DFG [25] or QCL sources [26].

For environmental monitoring, one of the main challenges of operating in the 3.3 μm region of the mid-infrared is choosing an absorption line that isn't subject to interference from atmospheric water vapour.

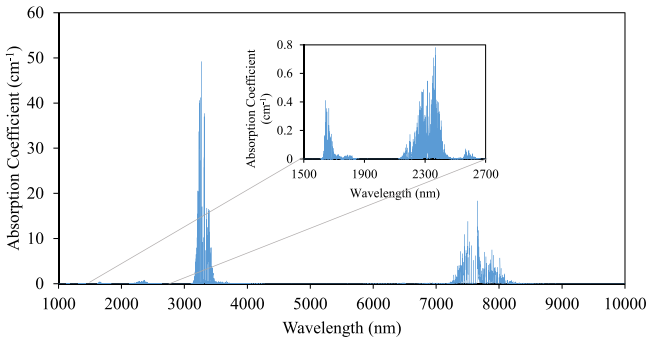

Fig. 1. Absorption spectrum for 100 % methane in the near and mid-infrared. Inset shows an expanded section of the spectrum centered around 2000 nm [27].

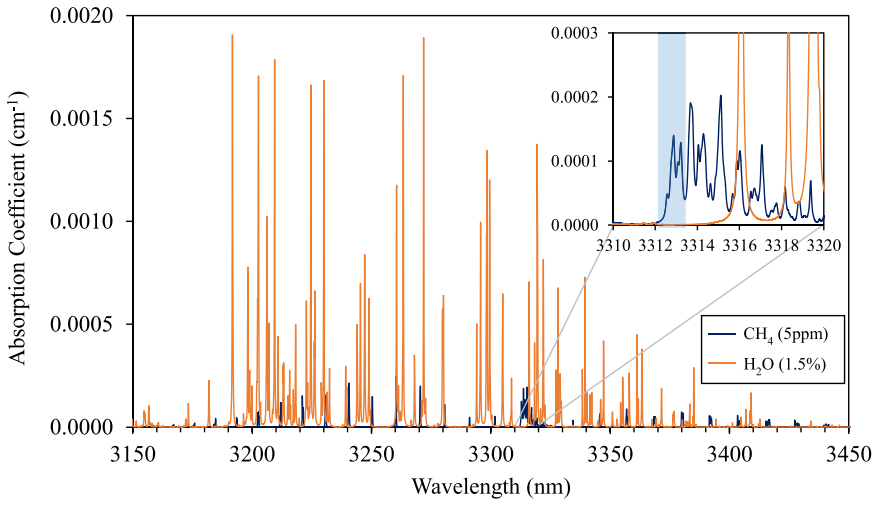

Fig. 2. Overlaid absorption spectra of 1.5 % water vapour (approximate atmospheric concentration at 25 °C and 75 % RH at sea-level) and 5 ppm methane, with the inset graph providing a closer view at the targeted wavelength region [27].

Fig. 2 shows the absorption lines for methane at 5 ppm and water vapour at 1.5 % (the approximate atmospheric concentration level at 25 °C and 75 % RH at sea-level, calculated using a psychrometric chart [28]). The graph demonstrates how a significant number of the strongest methane absorption peaks either overlap with, or are in close proximity to, a water absorption line. As a result, any absorption line used for atmospheric methane measurements has to be chosen carefully to avoid this interference.

The inset graph in Fig. 2 displays the absorption feature at 3313 nm chosen for analysis in this work, with a centre wavelength of the methane absorption far enough away from any water absorption to avoid interference. The complex nature of the chosen absorption feature, however, does present difficulties in the techniques used to measure it. The use of wavelength modulation spectroscopy on the feature would be difficult due to the number of lines present [29], especially as their linewidths would be affected by atmospheric pressure [30] and this would make calibration difficult [31]. Therefore direct spectroscopy was utilised for this work. Direct spectroscopy has the advantage of allowing measurement of the integrated absorption across a feature, this measure being more robust against changes of pressure [6].

3. Integrating spheres

Integrating spheres (or cavities) consist of a hollow container with a diffusely reflective internal surface. These cells are traditionally used for measuring the power output of an incident light source, however they have also been adapted for use as gas absorption cells, first by Venkatesh et al. in 1980 [32]. Typically, these cells possess two or more ports for light sources and detectors, with an additional two ports for gas inflow and exhaust. A light barrier (or baffle) is often positioned within the sphere to prevent direct illumination of the detector from the light source.

Integrating spheres have been shown to be tolerant to optical misalignment [6], allowing them to be utilised in conditions where high vibration levels and g-loading are present, such as those found on light aircraft. In contrast with other gas cells, integrating spheres do not produce structured interference fringes, reducing the amount of optimisation needed in their set-up. However they do suffer from speckle noise [22] and can be affected by optical feedback into the laser from diffuse reflections [33], which under certain conditions can create structured interference fringes or (from integrating spheres) high levels of spectral noise. Feedback from diffuse reflections is exacerbated by the collimation lens, which for back-reflected light can act as an efficient collector of feedback onto the laser chip. For operation at 1650 nm with DFB laser diodes, there are two remedies. First, we would require the use of an optical isolator between the laser and the integrating sphere to reduce the level of feedback. Second, a large optical pathlength between the laser and the diffuse reflector acts to reduce the free spectral range of the interference fringes such that they can be smoothed out by averaging or filtering [33]; this can be achieved using a source pigtailed to a sufficiently long length of fibre as sources are often available fibre-coupled. However, neither of these solutions was available in this work. Miniature isolators are not routinely available for mid-IR sources, ICLs are currently not packaged with fibre coupling and for our sensor there were significant space constraints; the only option was to place the laser as close as possible to the integrating sphere.

Pathlengths for these cells are typically of the order of a few metres in the near IR, with Tranchart et al. utilising a 4-inch diameter, Spectralon sphere with an effective pathlength of 4.4 m at 830 nm [20]. The achievable pathlength of an integrating sphere, however, is heavily dependent on the reflectivity of the surface, with reflective materials for the near infrared (Labsphere's Spectralon has a reflectivity of 99 % at 1650 nm) providing significantly longer pathlengths than those in the mid infrared. Fouling of the reflective surface can therefore also have a significant impact on pathlength, meaning that the surface reflectivity has to be monitored for changes [34].

For an integrating sphere, the surface radiance, B_s is given by [35].

$$B_s = \frac{\Phi_i}{\pi A_s} M \tag{3}$$

where Φ_i is the incident flux, A_s is the internal area of the sphere, and M is a dimensionless quantity known as the sphere multiplier. This multiplier accounts for the increase in radiance within the sphere due to multiple reflections and is given by

$$\boldsymbol{M} = \frac{\boldsymbol{\rho}}{\mathbf{1} - \boldsymbol{\rho}(\mathbf{1} - f)} \tag{4}$$

where ρ is the surface reflectivity and f is the port fraction, the fraction of the sphere surface area occupied by port openings. The average distance for each beam pass inside an integrating sphere is equal to two thirds of its diameter [36], meaning that the mean effective pathlength L_{eff} can be calculated to be

$$\boldsymbol{L_{eff}} = \frac{\mathbf{2}}{\mathbf{3}} \boldsymbol{DM} \tag{5}$$

where D is the diameter of the sphere and M is the multiplier described in Eq. (4). Using Eq. (5), a 4-inch diameter integrating sphere with an

Infragold [37] coated internal surface (95 % reflectivity at 3.3 μm) will have a theoretical effective pathlength of approximately 73.1 cm, using a port fraction of 0.04 giving a multiplier M equal to 10.8.

4. Method

Light from a collimated 3313 nm ICL (Nanoplus with collimator and heat sink) with a typical power of 2.3 mW was directed into a 4-inch diameter, Infragold coated integrating sphere (Labsphere 3 P-GPS-040-IG). The output from the collimator was coupled straight into one port of the integrating sphere without the need for additional coupling optics, or any additional gaps. The ICL was controlled to a temperature of 34.5 °C and driven with a sawtooth waveform at a frequency of 1 kHz using the output from a data acquisition system (16 bit National Instruments USB-6212 OEM multifunction DAQ) into a laser current driver / temperature controller (SRS LDC502), providing current tuning of ± 5 mA to give a wavelength range of approximately 1 nm. Two additional ports at 90° were used for gas inlet / outlet and for light detection. The diffusely reflected light was detected with an MCT (mercury-cadmium-telluride) photovoltaic detector (VIGO PV-2TE-4) cooled to −30 °C using a standard temperature controller (Wavelength Electronics HTC3000), with the signal amplified through a variable gain transimpedance amplifier (Femto DLPCA-200) at 10^6 V/A gain and 1.8 MHz bandwidth. This detector was chosen due to the size of its active area (0.1 × 0.1 mm, the largest available for this wavelength), its high detectivity at 3.3 μm (>3.0 × 10^{10} cm·$Hz^{1/2}$/W), and lack of immersion lens, which was not necessary for collection of diffusely reflected light from a wide surface area. The output was then fed to the same 16-bit computer-based data acquisition system with signal processing implemented in LabView, operating at 400 kS/s to provide 400 data points for each spectrum. In this manner, acquisition of a single spectrum was taken at 1 kHz and spectra were co-added over an averaging period of 1 s. A schematic diagram of this set-up is shown in Fig. 3, with a photo showing the relative positions of the sphere, laser and detector shown in Fig. 4.

To control the flow of methane and air being fed into the gas cell, cylinders containing methane and synthetic air (21.18 % O_2, <1 ppm CO_2, <2 ppm H_2O, <0.1 ppm NO_x, <0.1 ppm total hydrocarbon, balance N_2) were connected to a pair of mass flow controllers (Brooks Instrument model GF040CXX) regulated by a set point controller (Brooks Instrument 0254). Initially, a constant flow of gas from a cylinder containing 50.1 ppm methane in air was utilized to determine the correct current and temperature settings for the laser to align the absorption line

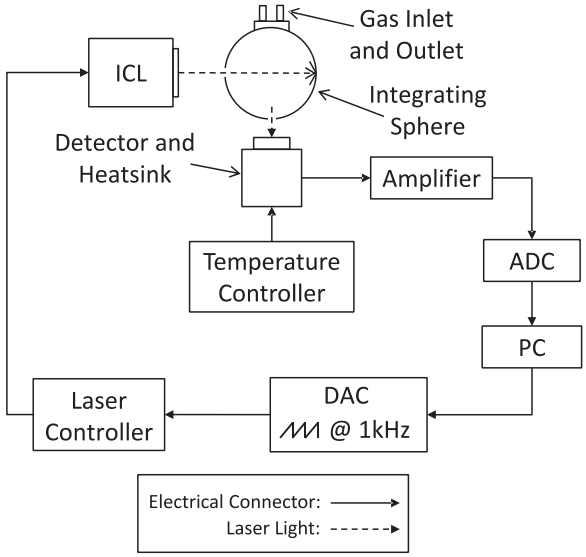

Fig. 3. Line diagram of experimental set-up using an integrating sphere.

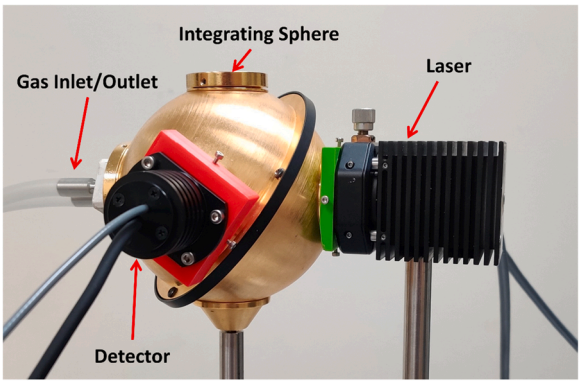

Fig. 4. Photo demonstrating the layout and relative positioning of the integrating sphere, ICL and detector. The integrating sphere allows for compact launch and detection optics (total size of integrating sphere, gas cell and detector 190×170×120mm), making the system suitable for use where space is at a premium.

with the centre of the waveform. Measurements were averaged over a 1 s period to reduce noise levels and using the Beer-Lambert law, shown previously in Eq. (2), values for the absorbance were calculated.

5. Experimental results

Fig. 5 shows a comparison between the raw data collected for a measurement of synthetic air and a measurement of 50 ppm methane in air, with the complex shape of the absorption clearly visible. As described previously, the Beer-Lambert law can then be applied onto these measurements to produce an absorbance curve. An example of the measurement at this methane concentration is shown in Fig. 6. When compared with data taken from the HITRAN database [27], also shown in Fig. 6, it can be seen that the detected methane absorption correlates strongly with this data. The wavelength scale of the measured absorption was correlated with the corresponding gas absorption on the HITRAN database. The noise seen in this data is a result of the system being detector noise limited.

The effective pathlength of the integrated sphere was estimated experimentally. By rearranging Eq. (2) to provide the pathlength, using the peak absorbance gained through the 50 ppm measurements and the absorption coefficient of 50 ppm methane at this wavelength, an effective pathlength of 70.1 cm was calculated. When rearranging Eqs. (4) and (5), this yields an average reflectivity value ρ of approximately 94.6 %, which is close to the manufacturer's specification of 95 %.

Measurements were then taken of the target absorption lines between 0 and 50 ppm methane concentrations. Using the effective pathlength to convert the methane measurements to Absorbance Units

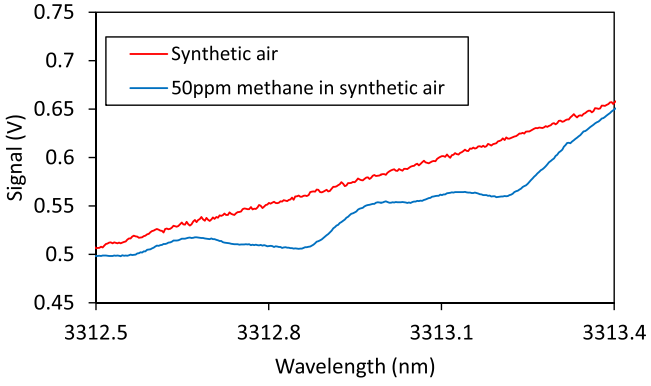

Fig. 5. Comparison between raw signals collected for synthetic air and 50 ppm methane.

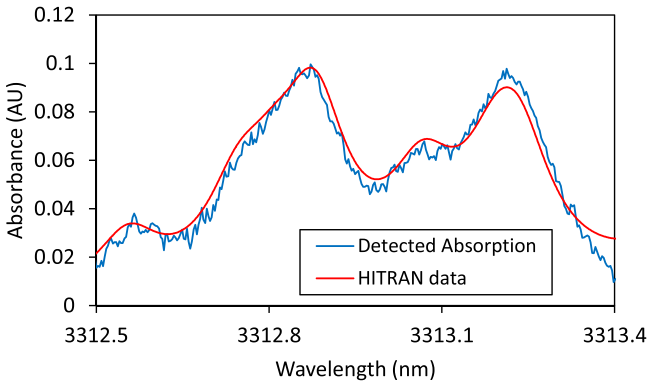

Fig. 6. Comparison between detected absorbance of methane at 50 ppm and the theoretical values from the HITRAN database (50 ppm at 25 °C and atmospheric pressure) [27].

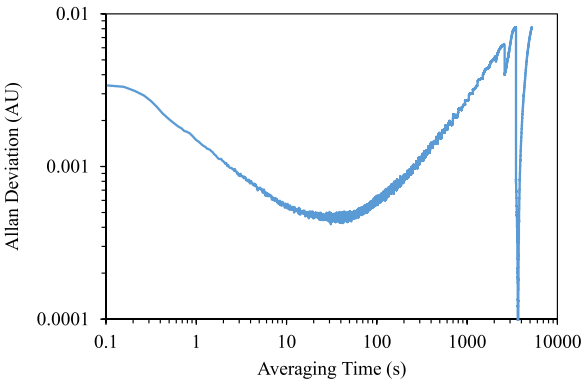

Fig. 8. Allan-Werle deviation plot for single point measurements displaying an NEA of 4.3 × 10^{-4} AU, corresponding to a methane concentration level of 220 ppb, at an averaging time of 40 s.

(AU), as described in Eq. (2), the peak absorbances of these measurements, corresponding to a single gas line at 3312.85 nm, were then plotted against their corresponding concentration, as seen in Fig. 7. The zero error was determined by comparing two measurements of synthetic air and taking the standard deviation. A value of 2.2 × 10^{-3} AU was produced for this measurement, which when compared against the peak absorbance at 50 ppm results in a single-point limit of detection of 1.1 ppm. Any deviation from linearity seen in this graph falls within the estimated experimental error, with the error bars shown being based on the fluctuations in the flow rate from the mass flow controllers and variations in the current and temperature controllers for the laser and detector.

Measurements of the noise in the system were made using a network signal analyzer (SRS SR780). Noise levels at a frequency of 1 kHz were determined to be 1.4 × 10^{-5} V·$Hz^{-1/2}$ for the detector (under dark conditions) and 1.5 × 10^{-5} V·$Hz^{-1/2}$ (with the laser also directed into the integrating sphere) and a DC signal level of 0.25 V. This yields an absorbance noise of 6.0 × 10^{-5} AU $Hz^{-1/2}$ for one measurement or 8.4 × 10^{-5} AU $Hz^{-1/2}$ where one measurement is subtracted from a second. These results indicated that the integrating sphere was largely detector noise-dominated, which is not surprising for a relatively lossy system.

We then need to consider the effective noise equivalent bandwidth (NEBW) of the system when collecting a spectrum consisting of 400 data points taken within a 1 ms period (2.5 μs per point). The equation for the NEBW has been given by Ingle and Crouch [24]:

$$NEBW = \frac{1}{2t_i} \tag{6}$$

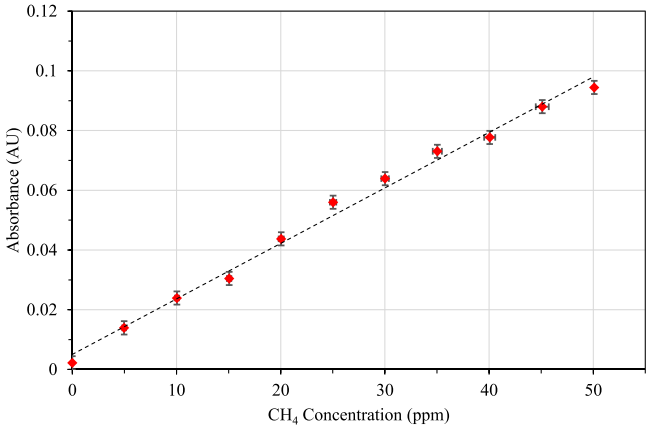

Fig. 7. Sensor measurements (single point at peak absorption) for methane concentrations between 0 and 50 ppm.

where t_i is the integration time. In this measurement, t_i is equal to the time period to measure an individual point (2.5 μs) multiplied by the number of spectra in an averaging period (1000 for a 1 s average), giving a NEBW of 200 Hz for a 1 s measurement and 10 Hz for a 20 s measurement. This yields single point noise equivalent absorbances of 1.2 × 10^{-3} AU and 2.7 × 10^{-4} AU for measurements over 1 s and 20 s respectively.

No evidence of optical feedback above the experimental noise was observed in the measurements.

An Allan-Werle deviation [38] was then constructed from measurements made over a 3-hour period by supplying the integrating sphere with a constant flow of 50 ppm methane at a flow rate of 100 cc/min (to overcome any possible fugitive leaks from the cell). The resultant Allan-Werle deviation plot for measurements at a single point (corresponding to the absorption peak) can be seen in Fig. 8, with an improved limit of detection of 220 ppb (absorption corresponding to 4.3 × 10^{-4} AU) at an averaging time of 40 s. Significant drift can be observed at longer averaging times, which is potentially a result of variations in the laser baseline over time.

To improve both the limit of detection and baseline stability, a non-linear least-square fit is performed utilizing a Levenberg-Marquardt algorithm. As the measurements are being undertaken at atmospheric pressure, the absorption line shapes and widths are determined primarily by collision induced broadening, which can be described using a Lorentzian function [39]. As such, seven evenly spaced Lorentzian peaks were used as the initial guess for the Levenberg-Marquardt line fit. The algorithm utilizes the results from the previous run as the initial values for the next data fit, with an estimate of the methane concentration being produced with each fit. An example of the resultant fit can be observed in Fig. 9. Using this technique, a limit of detection of 180 ppb could be achieved by determining the standard deviation for 20 fits of

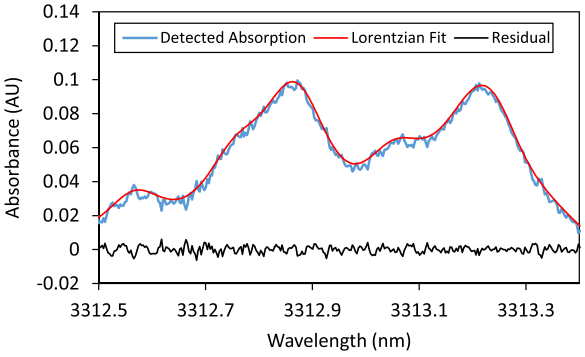

Fig. 9. Example of Levenberg-Marquardt line fitting algorithm applied to detected methane absorption at 50 ppm.

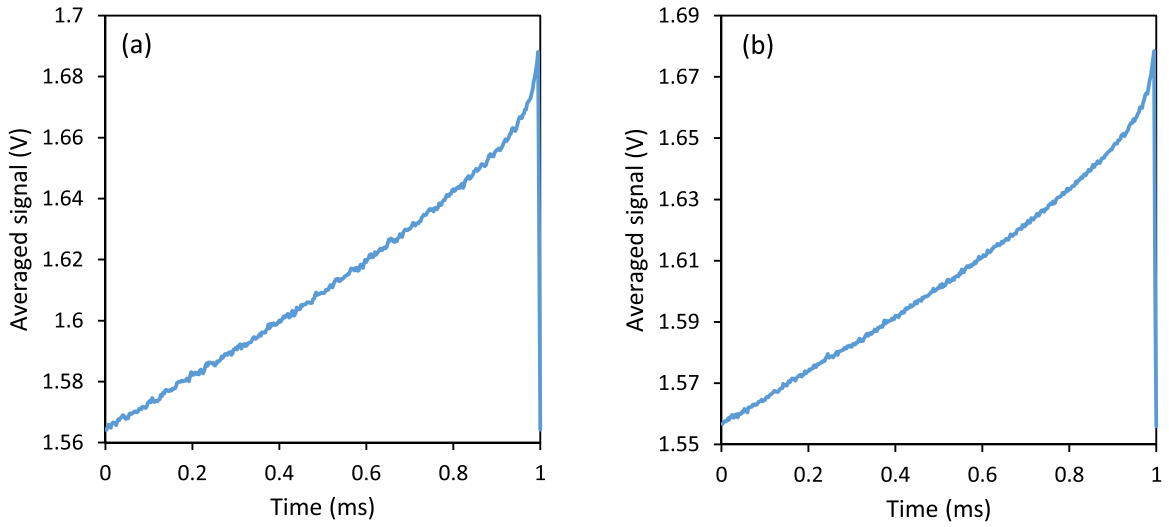

Fig. 10. Measured ramp waveforms, averaged over 10 s in the absence of methane, with the system under (a) normal operating conditions and (b) sustained vibration.

individual 1-second averaged absorption features, showing a small but notable improvement over the performance for a single data point.

During these experiments, we observed that the instrument was easy to align: as long as the incoming laser beam entered the cell through the entry port, the system was able to detect methane, with no observable change in performance for minor changes of beam path within the constraints of port size. We also observed that the measurements were robust against deliberate knocking of the cell and vibrations within the laboratory. This is consistent with the findings of Tranchart et al. for integrating spheres, who noted their tolerance to vibration and misalignment [20].

To confirm the system's tolerance to vibration, the integrating sphere, with the detector attached, was mounted on a shaker (Ling Dynamics V201) and allowed to move independently from the ICL. The same measurement conditions for the laser (34.5 °C, 1 kHz ramp modulation at ± 5 mA) and detector (−30 °C) that were used previously were applied. Vibration in aircraft can be attributed to low-frequency components caused by atmospheric turbulence, primarily occurring within a frequency range of 0.1 and 10 Hz [39], and higher frequency components up to 1 kHz [40]. Using this as a guide, for a preliminary measurement the shaker was set to vibrate sinusoidally at 15 Hz, 5 Vp-p. This combination of frequency and amplitude was chosen to generate a significant oscillation on the integrating sphere, producing approximately a 5 mm p-p fluctuation in the laser alignment, whilst also falling within the frequency ranges of the vibration expected on the light aircraft this instrument is designed to be mounted into.

Measurements were then taken of the detected ramp waveform for 10 s, both with the vibration present and without, both in the absence of methane so as to determine the baseline stability and noise. The resultant averaged waveforms can be observed in Fig. 10. The two measurements made have no appreciable difference in amplitude, with the measurements taken under vibration showing slightly improved noise levels. This demonstrates that system is tolerant to sustained vibration and misalignment.

To quantify the improvement in noise observed, a line fit was applied to the centre section of each ramp using a second order polynomial to account for the slight curvature in the measured signal. From this, the residuals of each curve could be calculated and subsequently plotted, as shown in Fig. 11. The standard deviations of these residuals are 5.8×10^{-4} V and 4.2×10^{-4} V for the normal operating conditions

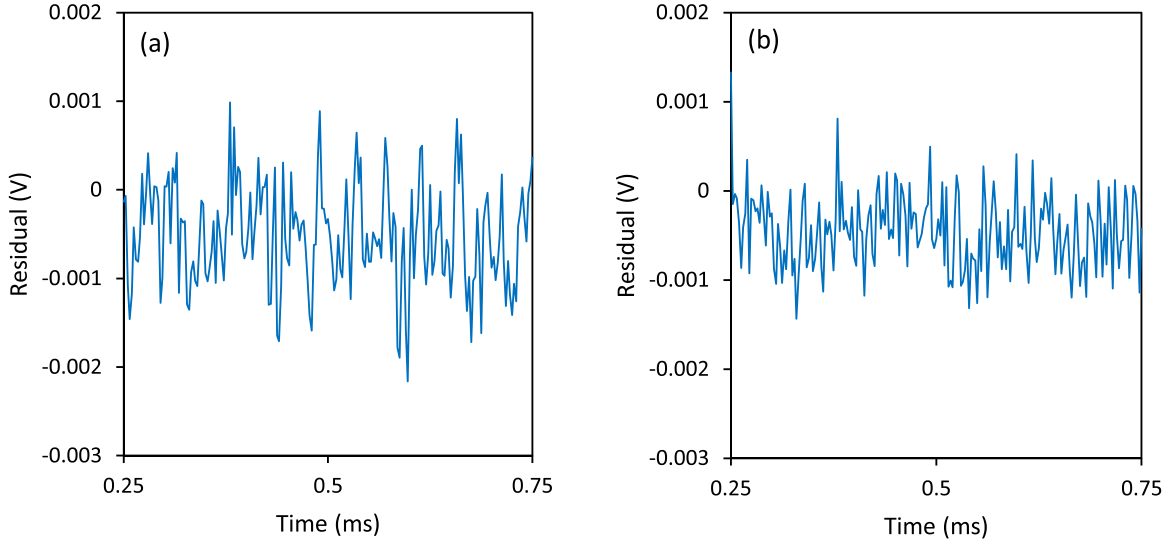

Fig. 11. Residuals from a second order polynomial line fit applied to measurements taken with the system under (a) normal operating conditions and (b) sustained vibration.

and sustained vibration measurements respectively.

6. Discussion and conclusions

Investigations were performed into the suitability of utilizing a mid-infrared interband cascade laser and integrating sphere for use in methane detection. The methane absorption feature at the chosen wavelength is complex, consisting of seven overlapping absorption lines, however the detected absorbance showed a good agreement with the theoretical values obtained from the HITRAN database. Measurements were then taken of methane concentrations between 0 and 50 ppm in 5 ppm steps, with the sensor response produced showing a good linearity, and any deviation falling within the estimated experimental error.

To determine the limit of detection of the system, a long-term repeatability test was performed by passing a sustained flow of 50 ppm methane into the integrating sphere over a period of 3 h. The resultant Allan-Werle deviation curve demonstrated a limit of detection of 220 ppb with an averaging time of 40 s for single point measurements, with a Levenberg-Marquardt line-fit improving this to 180 ppb for 20 fits of individual 1-second averages. This is a useful improvement over the expected performance using the same technology in the near IR, where absorption features are approximately 100 × smaller. Although the absolute performance is not as high as those seen in previous literature, when considering the small pathlength of the gas cell, the relative performance of the system is comparable (3.5×10^{-4} AU for the line fit limit of detection versus 8.1×10^{-4} AU for the system developed by Song et al. [7]). With the current background concentration of methane at 1.8 ppm, this limit of detection would allow for the measurement of fluctuations in this background level at a factor of 1 in 10, thus enabling the utilisation of this instrument for measurement of atmospheric levels whilst mounted in a light aircraft. If integrating spheres with longer pathlengths were developed, further improvements to the limit of detection could be achieved. For example, Cone et al. [41] have demonstrated a high-purity fumed silica powder with a reflectivity of 0.99919 at 532 nm, producing an effective pathlength of 41.15 m in a 5 cm diameter spherical integrating cavity.

The pathlength of the sphere, at 71 cm, does not compete with high quality multipass cells such as Herriott cells, but nevertheless does offer some advantages. Both the detector and laser were able to be positioned directly next to the integrating sphere ports. Our observations show that the alignment requirements for our system were minimal. A 5 mm p-p, 15 Hz oscillation applied to the integrating sphere and detector, moving them relative to the incident laser beam, displayed no measurable changes in the instrument readings, with preliminary measurements indicating a reduction in noise levels (standard deviations of the residuals decreasing from 5.8×10^{-4} V to 4.2×10^{-4} V) when a vibration is applied. Advantages therefore included ease of alignment, compactness, and minimising the effects of any background methane present in the optical path outside the gas cell. Despite the lack of isolator present in the system, no effects of feedback into the laser were observed.

Future work will involve the development and deployment of a compact version of the sensor to mount onto a light aircraft for application to environmental monitoring. Due to the tolerance to misalignment that is inherent with integrating spheres, it is anticipated that any vibrations or g-loading caused by the aircraft will have minimal effect on the performance of the instrument.

Funding

EPSRC EP/N002520/1, EP/R511511/1, NERC NE/K008307/1, Royal Society Paul Instrument Fund PI 120057.

CRediT authorship contribution statement

N Davis: Data curation, Formal analysis, Investigation, Methodology, Software, Validation, Visualization, Writing - original draft, review & editing, **D Francis:** Formal analysis, Investigation, Methodology, Software, Validation, **J Hodgkinson:** Conceptualization, Funding acquisition, Investigation, Methodology, Project administration, Resources, Supervision, Visualization, Writing - review & editing, **RP Tatam:** Funding acquisition, Investigation, Methodology, Project administration, Resources, Supervision, Writing - review & editing.

Declaration of Competing Interest

The authors declare that they have no known competing financial interests or personal relationships that could have appeared to influence the work reported in this paper.

Data availability

The data used in this article is provided in Cranfield Online Research Data (CORD) at https://doi.org/10.17862/cranfield.rd.22700626.

References

[1] IPCC, Summary for Policymakers, in: O. Edenhofer, R. Pichs-Madruga, Y. Sokona, E. Farahani, S. Kadner, K. Seyboth, A. Adler, I. Baum, S. Brunner, P. Eickemeier, B. Kriemann, J. Savolainen, S. Schlömer, C. von Stechow, T. Zwickel, J.C. Minx (Eds.), Climate Change 2014: Mitigation of Climate Change. Contribution of Working Group III to the Fifth Assessment Report of the Intergovernmental Panel on Climate Change, Cambridge University Press, Cambridge, United Kingdom and New York, NY, USA, 2014, pp. 1–33.

[2] IPCC, Summary for Policymakers, in: T.F. Stocker, D. Qin, G.-K. Plattner, M. Tignor, S.K. Allen, J. Boschung, A. Nauels, Y. Xia, V. Bex, P.M. Midgley (Eds.), Climate Change 2013: The Physical Science Basis. Contribution of Working Group I to the Fifth Assessment Report of the Intergovernmental Panel on Climate Change, Cambridge University Press, Cambridge, United Kingdom and New York, NY, USA, 2013.

[3] D.J. Wuebbles, K. Hayhoe, Atmospheric methane and global change, Earth-Sci. Rev. vol. 57 (3–4) (2002) 177–210.

[4] IPCC, Summary for Policymakers, in: V. Masson-Delmotte, P. Zhai, A. Pirani, S. L. Connors, C. Péan, S. Berger, N. Caud, Y. Chen, L. Goldfarb, M.I. Gomis, M. Huang, K. Leitzell, E. Lonnoy, J.B.R. Matthews, T.K. Maycock, T. Waterfield, O. Yelekçi, R. Yu, B. Zhou (Eds.), Climate Change 2021: The Physical Science Basis. Contribution of Working Group I to the Sixth Assessment Report of the Intergovernmental Panel on Climate Change, Cambridge University Press, Cambridge, United Kingdom and New York, NY, USA, 2021, pp. 3–32.

[5] G. Myhre, D. Shindell, F.-M. Bréon, W. Collins, J. Fuglestvedt, J. Huang, D. Koch, J.-F. Lamarque, D. Lee, B. Mendoza, T. Nakajima, A. Robock, G. Stephens, T. Takemura, H. Zhang, Anthropogenic and natural radiative forcing, in: T. F. Stocker, D. Qin, G.-K. Plattner, M. Tignor, S.K. Allen, J. Boschung, A. Nauels, Y. Xia, V. Bex, P.M. Midgley (Eds.), Climate Change 2013 the Physical Science Basis: Working Group I Contribution to the Fifth Assessment Report of the Intergovernmental Panel on Climate Change, vol. 9781107057, Cambridge University Press, Cambridge, United Kingdom and New York, NY, USA, 2013, pp. 659–740.

[6] J. Hodgkinson, R.P. Tatam, Optical gas sensing: a review, Meas. Sci. Technol. vol. 24 (1) (2013), 012004.

[7] F. Song, C. Zheng, D. Yu, Y. Zhou, W. Yan, W. Ye, Y. Zhang, Y. Wang, F.K. Tittel, Interband cascade laser-based ppbv-level mid-infrared methane detection using two digital lock-in amplifier schemes, Appl. Phys. B Lasers Opt. vol. 124 (3) (2018) 1–9.

[8] J. Xia, C. Feng, F. Zhu, S. Ye, S. Zhang, A. Kolomenskii, Q. Wang, J. Dong, Z. Wang, W. Jin, H.A. Schuessler, A sensitive methane sensor of a ppt detection level using a mid-infrared interband cascade laser and a long-path multipass cell, Sens. Actuators, B Chem. vol. 334 (September 2020) (2021), 129641.

[9] A. Sampaolo, S. Csutak, P. Patimisco, M. Giglio, G. Menduni, V. Passaro, F.K. Tittel, M. Deffenbaugh, V. Spagnolo, Methane, ethane and propane detection using a compact quartz enhanced photoacoustic sensor and a single interband cascade laser, Sens. Actuators B Chem. 282 (August 2018) (2019) 952–960.

[10] A. Sampaolo, P. Patimisco, M. Giglio, A. Zifarelli, H. Wu, L. Dong, V. Spagnolo, Quartz-enhanced photoacoustic spectroscopy for multi-gas detection: a review, Anal. Chim. Acta vol. 1202 (2022), 338894.

[11] K.M. Manfred, G.A.D. Ritchie, N. Lang, J. Röpcke, J.H. van Helden, Optical feedback cavity-enhanced absorption spectroscopy with a 3.24 μm interband cascade laser, Appl. Phys. Lett. vol. 106 (22) (2015), 221106.

[12] Y. Liu, Y. Ma, Advances in multipass cell for absorption spectroscopy-based trace gas sensing technology [Invited], Chin. Opt. Lett. vol. 21 (3) (2023), 033001.

[13] J.U. White, Long optical paths of large aperture, J. Opt. Soc. Am. vol. 32 (5) (1942) 285–288.

[14] D. Herriott, H. Kogelnik, R. Kompfner, Off-axis paths in spherical mirror interferometers, Appl. Opt. vol. 3 (4) (1964) 523.

[15] D.W. Ferguson, K.N. Rao, M.E. Mickelson, L.E. Larson, An experimental study of the 4-0 and 5-0 quadrupole vibration rotation bands of H2 in the visible, J. Mol. Spectrosc. vol. 160 (2) (1993) 315–325.
[16] C. Li, L. Dong, C. Zheng, F.K. Tittel, Compact TDLAS based optical sensor for ppb-level ethane detection by use of a 3.34μm room-temperature CW interband cascade laser, Sens. Actuators B Chem. vol. 232 (2016) 188–194.
[17] K. Liu, L. Wang, T. Tan, G. Wang, W. Zhang, W. Chen, X. Gao, Highly sensitive detection of methane by near-infrared laser absorption spectroscopy using a compact dense-pattern multipass cell, Sens. Actuators, B Chem. vol. 220 (2015) 1000–1005, https://doi.org/10.1016/j.snb.2015.05.136.
[18] J.B. Mcmanus, P.L. Kebabian, M.S. Zahniser, Astigmatic mirror multipass absorption cells for long-path-length spectroscopy, Appl. Opt. vol. 34 (18) (1995) 3336–3348.
[19] P. Werle, F. Slemr, Signal-to-noise ratio analysis in laser absorption spectrometers using optical multipass cells, Appl. Opt. vol. 30 (4) (1991) 430.
[20] S. Tranchart, I.H. Bachir, J.L. Destombes, Sensitive trace gas detection with near-infrared laser diodes and an integrating sphere, Appl. Opt. vol. 35 (36) (1996) 7070–7074.
[21] J. Hodgkinson, D. Masiyano, R.P. Tatam, Using integrating spheres as absorption cells: path-length distribution and application of Beer's law, Appl. Opt. vol. 48 (30) (2009) 5748–5758.
[22] D. Masiyano, J. Hodgkinson, R.P. Tatam, Gas cells for tunable diode laser absorption spectroscopy employing optical diffusers. Part 2: integrating spheres, Appl. Phys. B vol. 100 (2) (2010) 303–312.
[23] E. Hawe, P. Chambers, C. Fitzpatrick, E. Lewis, CO 2 monitoring and detection using an integrating sphere as a multipass absorption cell, Meas. Sci. Technol. vol. 18 (10) (2007) 3187–3194.
[24] J.D. Ingle, S.R. Crouch, Spectrochemical Analysis, Prentice Hall PTR,, New Jersey, USA, 1988.
[25] D. Richter, A. Fried, P. Weibring, Difference frequency generation laser based spectrometers, Laser Photonics Rev. vol. 3 (4) (2009) 343–354.
[26] B.-B. Zhao, X.-G. Wang, J. Zhang, C. Wang, Optical feedback effects on the relative intensity noise of a mid-infrared quantum cascade laser, Opt. Express vol. 27 (19) (2019) 26639–26647.
[27] I.E. Gordon, et al., The HITRAN2020 molecular spectroscopic database, J. Quant. Spectrosc. Radiat. Transf. vol. 277 (2022), 107949.
[28] M.A.I. El-Shaarawi, On the psychrometric chart, ASHRAE Trans. vol. 100 (1) (1994) 11–20.
[29] Z. Du, S. Zhang, J. Li, N. Gao, K. Tong, Mid-infrared tunable laser-based broadband fingerprint absorption spectroscopy for trace gas sensing: a review, Appl. Sci. vol. 9 (2) (2019) 1–33.
[30] G.B. Rieker, J.B. Jeffries, R.K. Hanson, Calibration-free wavelength-modulation spectroscopy for measurements of gas temperature and concentration in harsh environments, Appl. Opt. vol. 48 (29) (2009) 5546–5560.
[31] X. Zhao, P. Sun, Z. Zhang, Q. Wang, B. Wu, T. Pang, H. Xia, Q. Guo, M. Sun, Method for demodulating the overlapping absorption spectra of CO and CH4, Opt. Express vol. 30 (24) (2022) 43464.
[32] C.G. Venkatesh, R.S. Eng, A.W. Mantz, Tunable diode laser-integrating sphere systems: a study of their output intensity characteristics, Appl. Opt. vol. 19 (10) (1980) 1704–1710.
[33] D. Masiyano, J. Hodgkinson, S. Schilt, R.P. Tatam, Self-mixing interference effects in tunable diode laser absorption spectroscopy, Appl. Phys. B Lasers Opt. vol. 96 (4) (2009) 863–874.
[34] S. Bergin, J. Hodgkinson, D. Francis, R.P. Tatam, Integrating cavity based gas cells: a multibeam compensation scheme for pathlength variation, Opt. Express vol. 24 (12) (2016) 13647–13664.
[35] Labsphere. Technical Guide: Integrating Sphere Theory and Applications, Labsphere, New Hampshire, USA, 2017.
[36] J.T.O. Kirk, Modeling the performance of an integrating-cavity absorption meter: theory and calculations for a spherical cavity, Appl. Opt. vol. 34 (21) (1995) 4397.
[37] Labsphere, Infragold NIR-MIR Reflectance Coating. ⟨https://www.labsphere.com/product/infragold-nir-mir-reflectance-coating/⟩ (accessed Feb. 16, 2023).
[38] P. Werle, R. Mücke, F. Slemr, The limits of signal averaging in atmospheric trace-gas monitoring by tunable diode-laser absorption spectroscopy (TDLAS), Appl. Phys. B Photo Laser Chem. vol. 57 (2) (1993) 131–139.
[39] H.I. Schiff, G.I. Mackay, J. Bechara, The use of tunable diode laser absorption spectroscopy for atmospheric measurements, in: M.W. Sigrist (Ed.), Air Monitoring by Spectroscopic Techniques, Wiley, New York, 1994, pp. 239–334.
[40] N.J. Mansfield, G. Aggarwal, Whole-body vibration experienced by pilots, passengers and crew in fixed-wing aircraft: a state-of-the-science review, Vibration, vol. 5, no. 1, pp. 110–120, 2022.
[41] M.T. Cone, J.A. Musser, E. Figueroa, J.D. Mason, E.S. Fry, Diffuse reflecting material for integrating cavity spectroscopy, including ring-down spectroscopy, Appl. Opt. vol. 54 (2) (2015) 334–346.

Dr Nicholas Davis MInstP is a Research Fellow in Engineering Photonics at Cranfield, having previously completed his PhD in the Centre. He has several years' experience of the development of novel infrared spectroscopic instrumentation, including the use of novel tunable lasers, the instrument described in this paper, and a feasibility study to assess the potential for mid IR spectroscopic measurements to be made on asphalt in a standoff configuration.

Dr Daniel Francis MInstP is a Research Fellow in Engineering Photonics at Cranfield and previously completed his PhD in the Centre. His experience includes the development of novel speckle interferometry instrumentation for surface strain measurement of dynamic objects, mid-IR laser spectroscopy with hollow silica waveguides, and low-coherence interferometry for refractive index measurement.

Dr Jane Hodgkinson CPhys CEng MSPIE is a Reader in Applied Photonics within Engineering Photonics at Cranfield. In 2004 she established labs at Cranfield University for spectroscopic gas detection and leads this activity with funding from EPSRC, TSB/Innovate UK, NERC, the Royal Society and industry. She has published > 70 papers, has 8 granted patents plus 4 applications, and serves as the Chair of the Gas Analysis and Sensing Group, a UK-based technology forum.

Prof Ralph P Tatam DSc FInstP CPhys CEng CSci FSPIE has led Engineering Photonics at Cranfield since its inception in 1989 and holds a Personal Chair in Engineering Photonics ('98). He was awarded a DSc (Exeter University), made a Fellow of SPIE, the International Society for Optics and Photonics, and was elected to the SPIE Board of Directors. He has led research programmes supported by the EPSRC, EU, ATI, Innovate UK, Royal Society and a range of industrial organisations. He has published over 500 papers and patents

2023-04-23

Compact methane sensor using an integrating sphere and interband cascade laser at 3313 nm

Davis, Nicholas M.

Elsevier

Davis N, Francis D, Hodgkinson J, Tatam RP. (2023) Compact methane sensor using an integrating sphere and interband cascade laser at 3313 nm, Sensors and Actuators B: Chemical, Volume 389, August 2023, Article number 133866

https://doi.org/10.1016/j.snb.2023.133866